Phase Diagram of Spin States and Magnetic Interactions in Isotope Substituted $(Pr,Eu)_{0.7}Ca_{0.3}CoO_3$

A.V. Kalinov[1, 2, a], O.Yu. Gorbenko[3], A.N. Taldenkov[4], J. Rohrkamp[2],
O. Heyer[2], S. Jodlauk[2], N.A. Babushkina[4], L.M. Fisher[1], A.R. Kaul[3],
D.I. Khomskii[2], K.I. Kugel[5] and T. Lorenz[2]

[1]All-Russian Electrical Engineering Institute, Krasnokazarmennaya 12, 111250 Moscow, Russia

[2]II. Physikalisches Institut, Universität zu Köln, Zülpicher Str. 77, 50937 Köln, Germany

[3]Department of Chemistry, Moscow State University, 119991 Moscow, Russia

[4]Institute of Molecular Physics, Russian Research Center "Kurchatov Institute", Moscow, Russia

[5]Institute for Theoretical and Applied Electrodynamics, Izhorskaya Str. 13, Moscow, Russia

[a]kalinov@vei.ru

Abstract. The magnetic/spin-state phase diagram of the $(Pr_{1-y}Eu_y)_{0.7}Ca_{0.3}CoO_3$ series was obtained on the basis of measurements of the specific heat, thermal expansion, magnetization and resistivity. The phase diagram reveals three different states depending on the static distortions (Eu content), the oxygen-isotope mass, and the temperature. The samples with the lower Eu concentrations are ferromagnetically ordered up to moderate temperatures (about 50 K),, most probably, due to the low-spin Co^{4+} – intermediate-spin Co^{3+} interaction of the double-exchange type. As the Eu doping increases, the Co^{3+} LS ($S = 0$) state becomes stabilized and the magnetic ordering of the Co^{4+} ions is suppressed up to temperatures well below 5 K, resulting in a low-temperature anomaly in C_p. At higher temperatures, we observe a first-order spin-state transition from the LS to the IS state of Co^{3+}, which is accompanied by a decrease in the electrical resistivity, an increase in the magnetization, and a strong lattice expansion.

Introduction

Perovskite-based mixed-valence transition-metal (TM) oxides with the general formula $R_{1-x}A_xTM^{3+}_{1-x}TM^{4+}_xO_3$ (R = rare-earth, A = alkali-earth element) exhibit different ordering phenomena and phase transitions, e.g., antiferro- and/or ferromagnetic order, charge and/or orbital ordering, metal-insulator transitions [1] and a tendency to phase separation [2]. In addition to these phenomena common to most doped TM oxides, cobaltites have an extra "degree of freedom", namely, Co^{3+} ions in them can occur in different spin states: low-spin (LS; spin $S = 0$; $t_{2g}^6 e_g^0$), intermediate-spin (IS; $S = 1$; $t_{2g}^5 e_g^1$), or high-spin (HS; $S = 2$; $t_{2g}^4 e_g^2$) states, with spin-state transitions (SST) between them being influenced, e.g., by temperature, pressure, or doping [3]. Above T_{SST}, a higher spin state either IS or HS becomes thermally populated, affecting various physical properties, e.g., the magnetic susceptibility χ or the thermal expansion α. The susceptibility is obviously affected because the excited spin state (IS or HS) induces a significant increase in the magnetization. The thermal expansion is affected due to the different ionic radii: the smaller for LS Co^{3+} with empty e_g orbitals and the larger IS or HS Co^{3+} ions with partially filled e_g orbitals. The SST in $RCoO_3$ is strongly affected by both heterovalent and isovalent doping at the R site. The heterovalent doping ($R_{1-x}A_xCoO_3$; A = Ba, Sr, and Ca) causes a hole doping and stabilizes the magnetic (IS or HS) state of Co^{3+} [4]. The isovalent doping with the other (smaller) trivalent rare-earth ions, increases chemical pressure without changing the Co valence. In the latter case, the LS state of Co^{3+} ions is stabilized and the spin-state transition is shifted to a higher temperature [5]. Phenomena, for which the crystal lattice plays a significant role, usually show a strong isotope

effect, and vice versa studies of the isotope effect can yield important information about the underlying mechanisms [6]. Indeed, the first measurements [7] have already demonstrated the existence of an oxygen isotope effect in cobaltites with spin-state transitions.

Experiment and Results

Experimental Details. A series of $(Pr_{1-y}Eu_y)_{0.7}Ca_{0.3}CoO_3$ samples with $y = 0.12 – 0.26$ and ^{16}O, ^{18}O isotopes was synthesized by the "paper synthesis" technique. The chosen stoichiometries span the range of the mean rare-earth radius $\langle r_A \rangle$ from 1.172 Å to 1.164 Å, for $y = 0.12 – 0.26$. The end-member of this series, $Eu_{0.7}Ca_{0.3}CoO_3$, was also studied. Below, the samples are referred to as Eu_y-n, where y and $n = 16$ or 18 denote the Eu content and the oxygen isotope, respectively. The magnetization was measured in a vibrating sample magnetometer insert to a Quantum Design PPMS in the magnetic field range up to 14 T at temperatures 2 – 300 K. The electrical resistance R of the samples was measured using the four-probe technique (the two-probe method was used for $R > 1\ \Omega$) in the temperature range from 5 to 330 K. The specific heat C_p was measured using the Quantum Design PPMS by the two-tau relaxation technique from 2 to 300 K in magnetic fields up to 14 T. High-resolution measurements of the linear thermal expansion coefficient $\alpha = 1/L \cdot dL/dT$ were performed on heating from 4 to 180 K using a home-built capacitance dilatometer.

Results and Discussion. The results of measurements of thermal expansion α are shown in Fig. 1. Obviously, the data can be split in two groups: the "highly distorted" (HD) samples (larger y) show pronounced anomalies, which are almost completely absent in the "less distorted" (LD) samples. The borderline between the groups is located at $y_{th} = 0.18$ and depends on the oxygen isotope or, in other words, the (almost) absence or presence of this strong anomaly can be switched by exchanging the oxygen isotope from ^{16}O to ^{18}O. In Fig. 2 the specific heat measurements are illustrated. Again we observe the clear difference between the LD and HD samples. The HD samples show pronounced anomalies at temperatures which well agree with those of the corresponding anomalies in α. The shape of these anomalies is also rather symmetric as expected for a broadened first-order phase transition. In addition, there is a low-temperature upturn in C_p/T for all HD samples (as well as for the end-member $Eu_{0.7}Ca_{0.3}CoO_3$), which indicates the occurrence of another phase transition at $T < 2$ K, probably related to Co^{4+} ions ordering. The associated entropy [of about 1.2 J/(K·mol)] is quite comparable to the full magnetic entropy $\Delta S_{Co4+} = 0.3R \ln 2 = 1.73$ J/(K·mol) of Co^{4+} ions. The magnetic field of 10 T suppresses essentially the upturn (see inset to Fig. 2), giving evidence of a magnetic nature of this transition. Both these anomalies are absent for the LD samples.
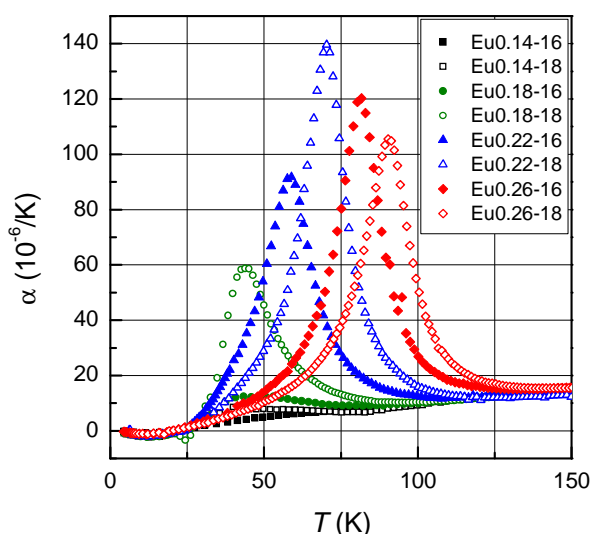

Fig. 1. Temperature dependences of the thermal expansion coefficient α.
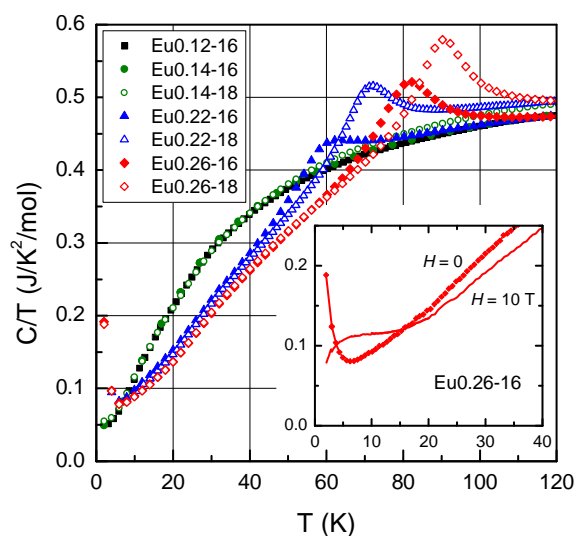
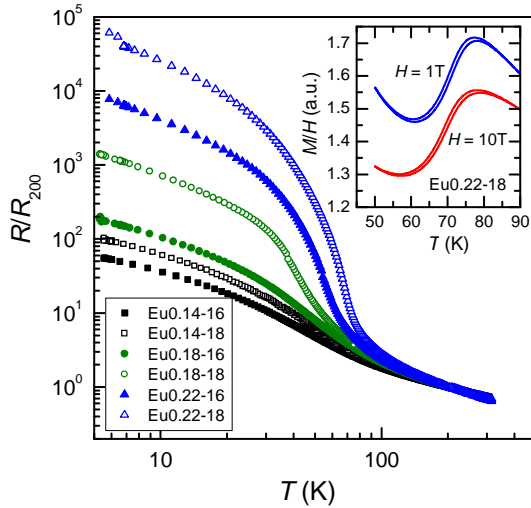Fig. 2. Temperature dependences of the specific heat C_p divided by temperature.

Fig. 3. Normalized resistivity as a function of temperature. The inset shows the normalized magnetization *vs.* temperature.

This spin-state transition is seen not only in the thermodynamic properties α and C_p but also in the electrical resistivity. The room temperature resistivity R_{200} is approximately the same for all the samples (about 10^{-3} $\Omega\cdot$cm) and the data presented in Fig. 3 demonstrate that it has a weak semiconducting behavior. Below 100 K, all the HD samples show a transition to a high-resistive state, which does not occur in the LD samples. The corresponding transition temperatures coincide well with the spin-state transition temperatures obtained in the thermal expansion and specific heat (Figs. 1, 2). There is also a distinct increase in the magnetization (see inset to Fig. 3) upon the transition, which supports the spin state transition to a higher spin state.

Based on all obtained results, we constructed the phase diagram describing magnetic and spin-state transitions (see Fig. 4). There are three magnetic/spin states of the Co^{3+} ions on the diagram. (Because we are not aware of any compound where Co^{4+} does not realize the LS state with $S = \frac{1}{2}$, only the spin state of the Co^{3+} ions is discussed.) In the HD samples (larger *y*), the Co^{3+} ions are in the LS state, and the transition to the IS state becomes possible with the temperature increase or with the decrease of the oxygen mass. Near the left border-line (hatched area) of this phase, the low-temperature magnetization achieves the saturation $M_s = 0.29$ μ_B, which is in a good agreement with the overall alignment of the Co^{4+} ions in the LS state. The magnetic ordering in this phase is not so well manifested. Most probably, there is some coexistence of the AFM and FM states, with the AFM ordering being more favorable for more distorted samples. Above the spin-state transition line (the IS state), there are still some traces of the FM ordering in the static magnetization data up to 150 K. Below about 5 K, there is an additional ordering (possibly of the Co^{4+} ions) marked by dotted area on the diagram.

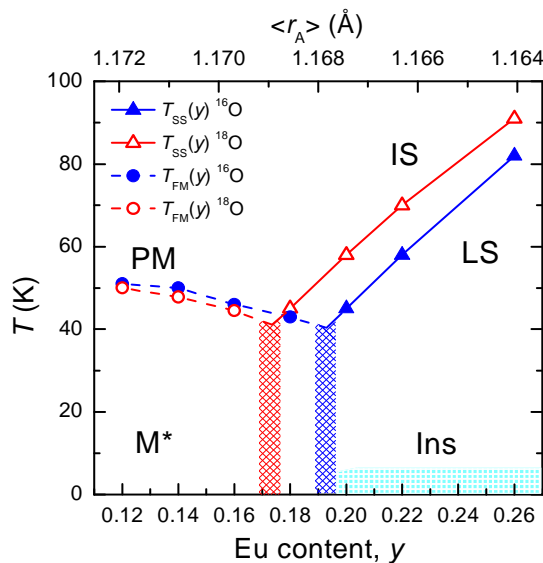For $y < y_{th}$ (LD state), the ground state becomes ferromagnetic with the large remanence and coercitivity. The fuzzy $T_{FM}(y)$ line separates it from the high-temperature paramagnetic IS state. For the Eu content just below y_{th}, the low-temperature saturation magnetization exceeds the maximum value for the LS state of all cobalt ions. This means that a certain portion of the Co^{3+} ions remains excited to the IS state down to the lowest temperatures, despite the extrapolation of the $T_{SS}(y)$ line to the low-*y* region goes well above these temperatures. This implies that in the absence of FM ordering, the Co^{3+} ions just below y_{th} would still be in the LS state. There is no upturn in the $C_p(T)/T$ data for this region, moreover the magnetic field of 10 T does not affect the specific heat at all. This suggests that the Co^{4+} ions are already ordered at high temperatures, giving rise to the coercitivity. The low-temperature resistivity in this state is lower by several orders of magnitude compared to the HD state, but there is no real metallicity in the $R(T)$ dependence. It could be related to the absence

Fig. 4. Magnetic/spin-state phase diagram. "PM", "M*", and "Ins" denote paramagnetic metallic, "bad metal", and insulating state, respectively.

of the "net" metallicity as well as the "net" ferromagnetism. The saturation magnetization reaches only 0.35 μ_B per Co site (up to 0.5 μ_B for the end-member $Pr_{0.7}Ca_{0.3}CoO_3$ [8]). The completely polarized Co^{3+} sublattice in the IS state should result in the much higher magnetization of 1.4 μ_B (and even more so for the HS state of all Co^{3+} ions). The $t_{2g}^5 e_g^1$ intermediate spin state makes the double exchange (DE) mechanism possible due to the presence of the itinerant e_g electrons that can explain the simultaneous nucleation of ferromagnetism and conductivity. We can qualitatively interpret these data (fuzzy transition, low magnetic moment, absence of a real metallic behavior) in the picture of a strongly inhomogeneous (phase-separated) state with the ferromagnetic metallic clusters embedded into the nonmagnetic and insulating (or, at least, less magnetic and less conducting) background. The increase of the temperature for the LD samples results in the smooth crossover to the paramagnetic state. This crossover is observable in Figs. 1, 2 as a broad hump in the temperature dependence.

The isotope-effect is clearly observed for the spin-state transition T_{SS}. The temperature T_{FM} has only marginal but visible dependence on the isotope content. However, for both phase boundaries [$T_{SS}(y)$ and $T_{FM}(y)$], the isotope exchange is equivalent to the change in y by approximately 0.02. This means that the static distortions due to the change in the mean ion-radius of rare-earth are somehow equivalent to changes in the lattice dynamics due to the isotope exchange, although the physical mechanisms are apparently different. An increase of Eu content leads to an increase of t_{2g}-e_g crystal-field splitting, which stabilizes the LS state. On the other hand, the main effect of the oxygen isotope substitution is the change of the effective intersite hopping, i.e., of the bandwidth.

Conclusion

The magnetic/spin state phase diagram of the $(Pr_{1-y}Eu_y)_{0.7}Ca_{0.3}CoO_3$ series was derived from the measurements of the specific heat, thermal expansion, magnetization and resistivity. The phase diagram reveals three different states depending on the temperature, static distortions (Eu content), and the oxygen-isotope mass. The samples with high Eu content exhibit the thermally activated spin-state transition. The samples with the lower Eu concentrations are ferromagnetically ordered below about 50 K due to the Co^{3+}-Co^{4+} double exchange, which favors the finite spin state of the Co^{3+} ions. With the Eu content increasing, the Co^{3+} LS state becomes stabilized and the magnetic ordering of the Co^{4+} ions is suppressed up to temperatures well below 5 K, making the spin-state transition to be driven merely by the temperature. The exchange of ^{16}O to ^{18}O shifts the phase boundaries to the lower Eu concentration, i.e., an increase in the oxygen mass acts similarly to an increase in the Eu content. We expect the regularities observed in these systems to be also applicable to other cobaltites with spin-state transitions.

References

[1] M. Imada, A. Fujimori, and Y. Tokura, Rev. Mod. Phys. **70**, 1039 (1998).

[2] M. Yu. Kagan and K. I. Kugel, Usp. Fiz. Nauk **171**, 577 (2001).

[3] M. A. Señarís-Rodríguez and J. B. Goodenough, J. Solid State Chem. **116**, 224 (1995).

[4] M. Kriener, C. Zobel, A. Reichl, *et al.*, Phys. Rev. B **69**, 094417 (2004).

[5] K. Berggold, M. Kriener, P. Becker, *et al.*, Phys. Rev. B **78**, 134402 (2008).

[6] N. A. Babushkina, L. M. Belova, O. Yu. Gorbenko, et al., Nature (London) 391, 159 (1998).

[7] G. Y. Wang, T. Wu, X. G. Luo, *et al.*, Phys. Rev. B **73**, 052404 (2006).

[8] S. Tsubouchi, T. Kyômen, M. Itoh, *et al.*, Phys. Rev. B 66, 052418 (2002).

Trends in Magnetism

Phase Diagram of Spin States and Magnetic Interactions in Isotope Substituted $(Pr,Eu)_{0.7}Ca_{0.3}CoO_3$